Soliton interactions between multivalued localized waveguide channels within ferrites

Francis T. Nguepjouo,[1,2,3,*] Victor K. Kuetche,[1,2,3,4,†] and Timoleon C. Kofane[2,3,4,‡]

[1]*National Advanced School of Engineering, University of Yaounde I, P.O. Box 8390, Yaounde, Cameroon*

[2]*Centre d'Excellence en Technologies de l'Information et de la Communication (CETIC), University of Yaounde I, P.O. Box 812, Yaounde, Cameroon*

[3]*Department of Physics, Faculty of Science, University of Yaounde I, P.O. Box 812, Yaounde, Cameroon*

[4]*The Abdus Salam International Centre for Theoretical Physics (ICTP), Strada Costiera, 11-I- 34151 Trieste, Italy*

(Received 5 October 2013; revised manuscript received 17 March 2014; published 16 June 2014)

In this paper, we investigate both analytically and numerically the localized multivalued waveguide channels—the loop solitons—dynamics within a ferrite slab. In the starting point of the work, we solve in detail the initial value problem of the system while unveiling the existence of multivalued waveguide channels solutions. Paying particular interest to the nonlinear scattering among these excitations, we study extensively the different kinds of interacting features between these localized waves alongside the depiction of their energy densities. As a result, we find that the interactions can be attractive or repulsive depending strongly on the ratio of the amplitudes of the interacting structures. In the wake of these results, we address some physical implications, accordingly.

DOI: 10.1103/PhysRevE.89.063201 PACS number(s): 41.20.Jb, 03.50.De, 05.45.Yv

I. INTRODUCTION

Nonlinear wave excitations and solitons—self-localized robust and long-lived solitary waves that do not disperse and preserve their identity as they travel through a medium—are ubiquitous in nature. Solitons actually result from the trade-off between nonlinearity (the tendency to increase the wave slope) and dispersion (the tendency to flatten the wave). They arise in many fundamental areas of physics and technology from high-bit-rate telecommunications and controllable soliton supercontinuum generation in ultrafast photonics, condensed matter, and plasma physics to elementary particle physics, cosmology, and monster (rogue) waves in oceans and Bose-Einstein condensates [1]. Because of their remarkable properties, the above waveguide channels might appear also as the idealized mathematical structures for the description of extended "elementary" particles [2,3]. This is the case of the new concept of optical leptons and the soliton models of the hydrogen atom investigated recently [4–6].

By virtue of the Galilean symmetry, the soliton as the self-localized wave object is characterized by its own analog of the de Broglie wavelength. On the other hand, the soliton as the extended particlelike object, due to the nonlinear self-interaction, becomes a bound state in its own self-induced trapping potential and, as a consequence, acquires a negative self-interaction (binding) energy [7,8]. With the soliton binding energy, ones can get details about the shape and the structural stability of solitons and, similarly to the nuclear binding energy, it can be regarded as the degree of how strongly the quasiparticles that make up the soliton are bound together.

From the viewpoint of their profiles, solitons can be classified into two families: the single-valued waveguide channels and the multivalued waveguide channels. The latter have recently been investigated experimentally in a variety of physical systems such as vortex lines of fluid dynamics [9–11], topological defect lines in liquid crystals [12,13], singular lines of optical fields [14], magnetic field lines in electromagnetic fields [15–17], and in spinor Bose-Einstein condensates [18], just to name a few. Nonetheless, the analytical tools designed to capture these intricate structures have remained, until now, a challenging problem to investigate. In few months ago, some complex multivalued excitations have been unearthed in the light fields analytically by Kedia *et al.* [19] as a new family of null solutions to Maxwell's equations in free space whose field lines encode all torus knots and links. The loop solitons [20] alongside the twofoil and trefoil strings can be regarded as simple reductive cases of these kinds of multivalued excitations. We aim at investigating the nonlinear dynamics of such structures in the ferrite materials and project to extend the study to the construction of more complex multivalued solitons of knot profiles. The motivation of the present paper also stems from the contemporary interests in studying loop soliton solutions to integrable nonlinear evolutionary equations (see Ref. [21] and references therein).

Following the increasing interests in advanced magnetic information storage and data process elements, it becomes fundamental and more crucial to understand deeply the micromagnetic structure in microsize and nanosize of magnets among the ferromagnetic materials [22–25]. Some developed nanofabrication techniques have made it possible to fabricate ferromagnetic particles to a length of 20–30 nm [22]. Due to the relatively small size of such nanoparticles, the magnetization can be regarded as homogeneous over a particle and can be described by a magnetic moment. These particles interact with each other through a dipolar interaction of the magnetic moments and the solitons originating from this interaction are stably created. Alongside these structures, a wide range of soliton-type propagation phenomena have been predicted theoretically (see Refs. [26–28] and references therein).

In the past few years, there has been extensive research activity on dissipative magnetization dynamics (see Ref. [29] and references therein) in view of understanding some technological problems for magnetic materials. This research activity aimed to reduce energy losses due to damping and also to developing materials with higher rates of magnetization, determined, however, by damping mechanisms. The dissipative magnetization dynamics of a ferromagnet can be subdivided

*nguepjouofrancis@yahoo.fr
†vkuetche@yahoo.fr
‡tckofane@yahoo.com

into fast and ultrafast processes. In the fast one, the slow magnetic degrees of freedom are investigated on a time scale much larger than the intersite hopping time of about 1 fs. For such a time scale, the dynamics are closed to the adiabatic limit where the electronic system is always in its ground state within the momentary magnetization configuration. As a matter of fact, in several films of nm thickness, spin-polarized current-induced switching of the magnetization direction has been observed [30,31]. Ultrafast dynamics occur on shorter time scales, e.g., the quenching of ferromagnetic order in about 100 fs [32]. In this work, we will restrict our interest to the fast near-adiabatic magnetization dynamics which stand to be the basic mechanism of the process of remagnetization in ferromagnetic materials.

Basically, the understanding of the electromagnetic propagation in ferromagnetic materials is actually made possible by the Maxwell's equations in such media. Theses equations are supplemented with a relation between the magnetization and the auxiliary magnetic field in the materials. Such a relation appears as the phenomenological equation of motion for the magnetization. A physical description of the micromagnetic phenomena is based on the use of the Landau-Lifshitz-Gilbert (LLG) equation controlling the magnetic relaxation process and determining how fast the magnetization is restored to its equilibrium position [29]. As far as we are concerned, no fully analytical theory has been developed so far to solve the above equations. Nonetheless, in view of obtaining results valid in nonlinear regimes, one has to resort to intermediate models where a novel perturbative parameter, most often of longness or shortness of the wave, is introduced [33].

In the present paper, we pay attention to the propagation of short waves in a saturated ferrite only in the direction perpendicular to the external saturating magnetic field. Granted this consideration is satisfied, the nonlinear dynamics actually obey an evolution system which integrability can be investigated by means of the phase portrait analysis combined to the Hirota's bilinearization [34] among other methods of study. The initial value problem of the system provides a whole depiction of the dynamics of the system while revealing the existence of miscellaneous traveling waveguide excitations supported by the system. The Hirota's bilinearization [34] provides a whole analysis of the interaction of localized waves while characterizing the head-on collision.

In the wake of the above concerns, we organize the paper as follows. In Sec. II, we present the basic nonlinear system consisting of two coupled evolution equations derived from the Maxwell's equations combined to the LLG phenomenological theory of damping in ferromagnets [29]. This basic system governs the propagation of nonlinear electromagnetic short waves within the ferrites [26]. In Sec. III, we solve the initial value problem of the system while depicting its phase portraits alongside the energy densities of the traveling waveguide channels. This analysis reveals the existence of localized and periodic traveling excitations propagating within the medium. In Sec. IV, paying particular interest to the localized waves, we investigate their scattering properties by means of the Hirota's bilinearization [34] and we also depict the energy functional of the waves. In Sec. V, we address the physical implications of the solutions. Finally, in the last section, we end this work with a brief summary.

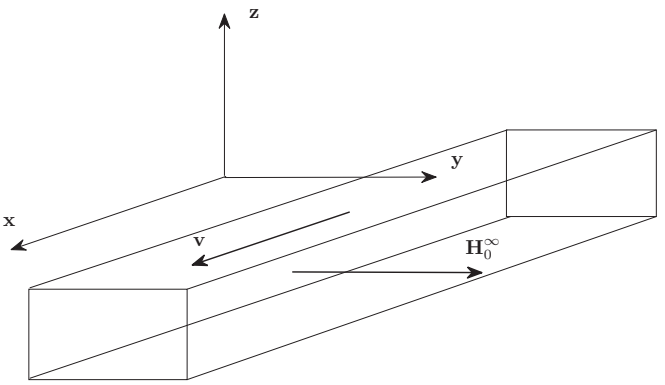

FIG. 1. Configuration considered. Vectors **v** and $\mathbf{H}_0^\infty$ stand for the velocity of the wave propagation and the in-plane external magnetic field, respectively.

II. BASIC NONLINEAR SYSTEM

We consider a quasi-one-dimensional ferrite slab lying in the x axis, the transverse dimension being negligible. This slab is magnetized to saturation by an in-plane external field $\mathbf{H}_0^\infty$ directed along the transverse y axis perpendicular to the propagation x direction as presented in Fig. 1. In such a condition, due to the absence of eddy currents, electromagnetic waves are likely to propagate. We consider a thick-enough film in view of ensuring an homogeneous magnetization over the ferrite. We assume that the crystalline and surface anisotropy of the sample is negligible. The use of the Maxwell's equations combined to the LLG equation [29] for a ferrite result in the derivation of the following dimensionless coupled system [26]:

$$-\nabla\cdot(\nabla\cdot\mathbf{H})+\Delta\mathbf{H}=\partial_t^2(\mathbf{H}+\mathbf{M}), \tag{2.1a}$$

$$\partial_t\mathbf{M}=-\mathbf{M}\wedge\mathbf{H}_{\text{eff}}+\sigma\mathbf{M}\wedge\partial_t\mathbf{M}/m, \tag{2.1b}$$

where the vectors **H** and **M** stand for the dimensionless magnetic induction and magnetization density, respectively. From a practical viewpoint, the above coupled equations are actually fundamental for investigation of the data loading processes in reversal magnetic memory devices in the ferrites. We note that the independent space-time variables are expressed into their dimensionless forms. The constants m and σ refer to the dimensionless saturation magnetization and Gilbert-damping parameter [29], respectively. Generally speaking, damping of a physical system generates a force in opposition to the macroscopic driving force. When the two forces balance, the energy gain from the driving force is balanced by the energy loss from the damping force while leading to a steady state. When the forces are not equal, energy is either gained (if the driving force is larger) or lost (if the damping force is larger), and the macroscopic motion either accelerates or decelerates. If the damping force always increases or decreases as the rates of change of the dynamical variables that characterize the macroscopic motion increase or decrease, then when the driving force is constant, the rates of change of the dynamical variables increase or decrease until the driving and damping forces are equal and a steady-state condition is attained. The simplest case, which commonly occurs when there are many

different damping forces out of any resonance phenomenon, is that the damping force is directly proportional to the rate of change of the macroscopic dynamical variables of the system [29].

Now, considering a uniaxial ferrite referring to a quasi-one-dimensional configuration presented in Fig. 1 above, we use the following expansion series of the magnetization density and the magnetic induction expressed as [26]:

$$\mathbf{M} = \sum_{j=0}^{\infty} \mathbf{M}_j \epsilon^j, \quad \mathbf{H} = \sum_{j=0}^{\infty} \mathbf{H}_j \epsilon^j, \tag{2.2}$$

where the parameter ϵ represents the small perturbation related to the wavelength of the short-wave perturbation along the ferrite. Replacing Eq. (2.2) into (2.1) and following a blend of transformations where two independent space-time coordinates X and T express [26]

$$X = -\epsilon^{-1} m(x - t)/2, \quad T = \epsilon m t, \tag{2.3}$$

Eq. (2.1) transforms to

$$B_{XT} = BC_X - sB_X, \tag{2.4a}$$

$$C_{XT} = -BB_X, \tag{2.4b}$$

where observables B and C and constant s are defined by [26]

$$C = -X - \int^X \left(\mathrm{H}_0^{\mathrm{y}}/m\right) dX, \quad B = \mathrm{M}_1^{\mathrm{x}}/2m, \quad s = -\sigma_1/2. \tag{2.5}$$

Let us note that, conventionally, subscripts to observables with respect to the space-time variables refer to their partial derivatives. Thus, from the above equations, writing B_X or C_X, for example, means the partial derivatives of observables B and C with respect to variable X. Besides, we need to mention that the dependent functions B and C expressed above represent the "relative magnetization" of the ferrite [26] with respect to the saturation magnetization and the "integral effective magnetic strength" of the ferrite, respectively. Parameter σ_1 stands for the first-order expansion cœfficient of the dimensionless Gilbert damping against the short-wavelength perturbation. The quantities H_0 and M_1 instead, refer to the zeroth and first-order expansion coefficients of the external magnetic field and the magnetization, respectively. According to Eq. (2.4), these observables evolve dynamically within the space-time-like manifold described by variables X and T, respectively, with the boundary conditions $\lim_{X\to\infty} \mathbf{H}_0 = (0,\mu m,0)$ and $\lim_{X\to\infty} \mathbf{M}_1 = 0$, parameters m and μ ($\mu > 0$) being the saturation magnetization and strength of the internal magnetic field of the ferrite, respectively [26]. For the sake of simplicity, these two independent variables will be written into their lower cases x and t, respectively.

The term $(-sB_X)$ in Eq. (2.4a) accounts for the Landau-Gilbert damping, which represents the dissipation which occurs in a real ferrite. Let us provide an explanation regarding where the absorbed energy of a damped ferromagnet comes from. First, we need to note that for a ferromagnet, as it is the case for ferrites in this paper, the dynamical characteristic observable is the magnetization field. In such materials, the damping involves loss of energy from the macroscopic motion of the local magnetization field by transfer of kinetic and potential energies to microscopic thermal motion (heat energy) in the form of spin waves, lattice vibrations (phonons), and thermal excitations, among others. However, the details of the mechanisms for the transfer processes are too complex to be taken into account explicitly in the field equations. Nonetheless, when the external magnetic field is not strong enough to eliminate all domain walls, the domain structure plays a dominant role in the damping, and the local rate of energy loss vary by large amounts within a ferromagnet [29].

It is of particular interest to see that the effects of the Gilbert-damping account significantly at the first order of expansion in the perturbative reduction method: $\sigma \sim \sigma_1\epsilon + O(\epsilon^2)$. In some typical materials, keeping only the second-order expansion coefficient ($\sigma \sim \sigma_2\epsilon^2$) discards the dissipation in the final analysis. This is actually of good interest when investigating the dynamics of self-confined coherent structures propagating in the ferrite with conserved properties such as shape, amplitude, and momentum, just to name a few. As a matter of fact, for vanishing dissipation parameter $s \equiv 0$, a soliton solution to Eq. (2.4) has been obtained by Kraenkel, Merle, and Manna [26] via a transformation to the sine-Gordon (sG) equation and given by

$$B = 2\frac{(1+\mu)}{\overline{\kappa}}\mathrm{sech} Z,$$

$$C = -(1+\mu)\left(X - \frac{2}{\overline{\kappa}}\tanh Z\right) + C_0, \tag{2.6}$$

where the phase z is given by

$$Z = \overline{\kappa} X - \frac{1+\mu}{\overline{\kappa}} T + Z_0, \tag{2.7}$$

with wave number $\overline{\kappa}$ and constant C_0 and Z_0 being arbitrary parameters. Following such a transformation, it is actually difficult to discuss in detail the interacting features of two-soliton, three-soliton, and multisoliton solutions due to some cumbersome calculus. In this work, we propose an alternative and interesting approach to study these waves in detail, i.e., to describe the sG solitons.

In the wake of the derivation of the aforementioned coupled equations, from the viewpoint of integrability, it is always straightforward to investigate whether such a system would possess an infinite set of conservation quantities. One powerful and direct method addressed to study this subject is the initial value problem resorting to the Hirota's bilinearization [34].

III. PHASE PORTRAIT ANALYSIS

Let us pass to a global coordinate in which the system (2.4) has stationary solutions. In this consideration, we introduce the following variable η given by

$$\eta = x - vt + \eta_0, \tag{3.1}$$

where the quantity η_0 is an arbitrary parameter and the nonzero constant v here stands for the velocity of the traveling waves. Setting $B(x,t) = \phi(\eta)$, $C(x,t) = \psi(\eta)$, the system (2.4) transforms to

$$v\phi_{\eta\eta} + \phi\psi_\eta - s\phi_\eta = 0, \tag{3.2a}$$

$$v\psi_{\eta\eta} - \phi\phi_\eta = 0. \tag{3.2b}$$

As mentioned previously, subscripts to observables ϕ and ψ with respect to sole coordinate η denote their total derivatives, accordingly. From Eq. (3.2b), after the first integration with respect to variable η, it straightforwardly yields

$$\psi_\eta = \phi^2/2v + K, \tag{3.3}$$

with K being an arbitrary parameter. The physical meaning of the parameter K is quite straightforward. In fact, comparing Eqs (2.5) and (3.3) from the viewpoint of their asymptotical behaviors provides $K = -(1+\mu)$ which stands to be negative valued ($\mu > 0$). It can be interpreted as the "effective saturation internal magnetic strength" of the ferrite.

From a physical viewpoint, according to Eq. (2.5), the dependent variable ϕ represents the "relative magnetization" of the ferrite [26] with respect to the saturation magnetization. To provide a physical meaning of the variable ψ, let us first mention that $\lim_{X\to\infty} C_X = -(1+\mu)$, which can be interpreted as the "effective saturation internal magnetic strength" of the ferrite. Thus, with the expression of the dependent variable C given by Eq. (2.5), the variable ψ can be construed as the "integral effective magnetic strength" of the ferrite at a given time of the dynamics towards the saturation regime.

From Eq. (3.2), we can easily derive the Hamiltonian-like of the system as follows: Multiplying Eq. (3.2a) by $(-\phi_\eta)$ and taking into account the expression given by Eq. (3.3) provides

$$(-v/2)\partial_\eta\left[\phi_\eta^2 + (K + \phi^2/2v)^2\right] = -s\phi_\eta^2. \tag{3.4}$$

It is hence straightforward to define the Hamiltonian-like of the system as

$$\mathcal{H} = -v\left[\phi_\eta^2 + (K + \phi^2/2v)^2\right]/2, \tag{3.5}$$

provided the following relation:

$$\mathcal{H}_\eta = -s\phi_\eta^2 \tag{3.6}$$

is satisfied.

We need to mention that by "system" we mean the nonlinear coupling of the external magnetic field and the magnetization of the ferrite which dynamics are described by Eq. (2.4). Due to the fact that the variable η does not appear explicitly in Eq. (3.5), from a physical viewpoint, the system is natural and the Hamiltonian refers to its "energy." We note that this "energy" given by the Hamiltonian needs to be construed as the energy of the traveling waveguide excitations supported by the system under interests. It is actually clear that this "energy" is not identical to the energy of the physical system.

From Eq. (3.5), as the traveling waves are moving, their "energy" decreases with η. Thus, it appears that waves moving toward the positive direction of the propagating axis are more stable than those traveling to the left-hand side of the axis.

As mentioned previously, due to the fact that the system under interest is natural, the above Hamiltonian-like expression actually stands for its total energy. Its kinetic-like $\mathcal{T}$ and potential-like energy $\mathcal{V}$ are expressed as

$$\mathcal{T} = -v\phi_\eta^2/2, \quad \mathcal{V} = -v(K + \phi^2/2v)^2/2, \tag{3.7}$$

showing a typical ϕ-four potential type in which the traveling waveguide channels are dynamics. We note that for $s = 0$, the energy of the system is constant as we will see in the figures.

In addition, from Eq. (3.7), the Lagrangian-like $\mathcal{L} = \mathcal{T} - \mathcal{V}$ of the system above is expressed as

$$\mathcal{L} = -v\left[\phi_\eta^2 - (K + \phi^2/2v)^2\right]/2. \tag{3.8}$$

According to the Euler-Lagrange formalism for real mechanical system dynamics submitted to conservative and nonconservative constraints, the equation of motion of such systems reads as follows:

$$\frac{\delta\mathcal{L}}{\delta\phi} = \frac{\partial\mathcal{L}}{\partial\phi} - \frac{d}{d\eta}\left(\frac{\partial\mathcal{L}}{\partial\phi_\eta}\right) = -F_{\rm nc}, \tag{3.9}$$

where the quantity $F_{\rm nc}$ stands for the nonconservative external constraint acting on the system. It is expressed as

$$F_{\rm nc} = -s\phi_\eta. \tag{3.10}$$

From the above expressions, the Hamilton equations are given by

$$\frac{\partial\mathcal{H}}{\partial p} = \phi_\eta, \quad \frac{\partial\mathcal{H}}{\partial\phi} = F_{\rm nc} - p_\eta, \tag{3.11}$$

where the quantity p refers to the conjugate momentum to the observable ϕ. According to the Euler-Lagrange formalism above, the conjugate momentum expresses $p = \partial\mathcal{L}/\partial\phi_\eta \equiv -v\phi_\eta$. Defining a variable y while setting

$$p = -vy, \tag{3.12}$$

the system (3.11) becomes

$$\phi_\eta = y, \quad y_\eta = \left[-\phi(K + \phi^2/2v) + sy\right]/v, \tag{3.13}$$

from which, using the four-order Runge-Kutta computational scheme, one can seemingly discuss the phase portrait features of the system. We aim at paying particular interest to the dynamics of the observable ϕ. Accordingly, from Eq. (3.13) it is straightforward that on all points of the axis $y = 0$, the orbits cross the axis perpendicularly. Also, on all points of the curve $-\phi(K + \phi^2/2v) + sy = 0$, the orbits possess horizontal tangents.

From a physical viewpoint, in order to investigate the genuine meaning of the variable y, we need to consider the equation giving the expression of the z component of the external magnetic field H_0^z as $H_0^z = -mB_X$ derived by Kraenkel, Merle, and Manna [26]. Incidently, it comes that $y = -H_0^z/m$. Hence, the variable y appears as the "relative z component of the zeroth-order (with respect to the wavelength perturbation) external magnetic field" of the ferrite with respect to the saturation magnetization. It can also characterize the "internal magnetic strength along the transverse z direction."

In order to properly manage the numerical investigation of the above coupled system, it is actually important to start off with the full analytical survey of its dynamical features around the equilibrium point by means of the Lyapunov method.

The equilibrium point of the system (3.13) is derived from the system

$$\phi(K + \phi^2/2v) = 0, \quad y = 0. \tag{3.14}$$

Since the product Kv is negative valued, the system (3.13) presents three equilibrium points (0,0), (ϕ_0,0), where

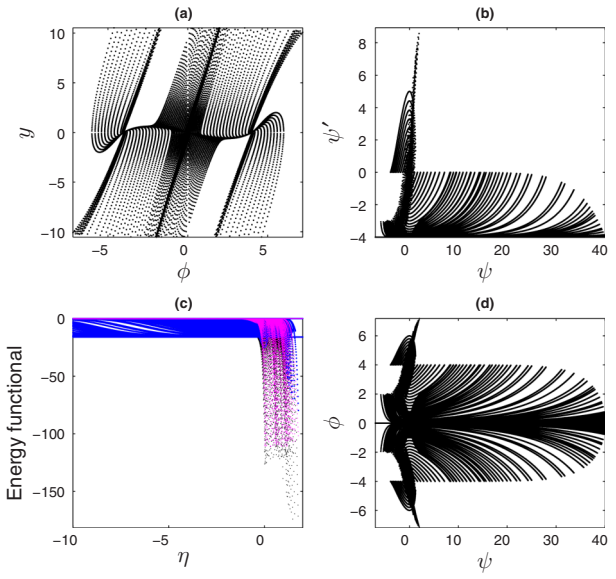

FIG. 2. (Color online) Phase features and energy functional of the system (3.13). The upper panels (a) and (b) depict the phase portraits of the system and the lower panel (c) deals with the energy densities of the corresponding traveling waveguide channels with the velocity $v = 2$ within a dissipation $s = 10$ and $K = -4$. In this panel, black, blue, and magenta represent the total energy, the potential energy, and the kinetic energy of the waves, respectively. Panel (d) presents the variations of observable ϕ with respect to ψ.

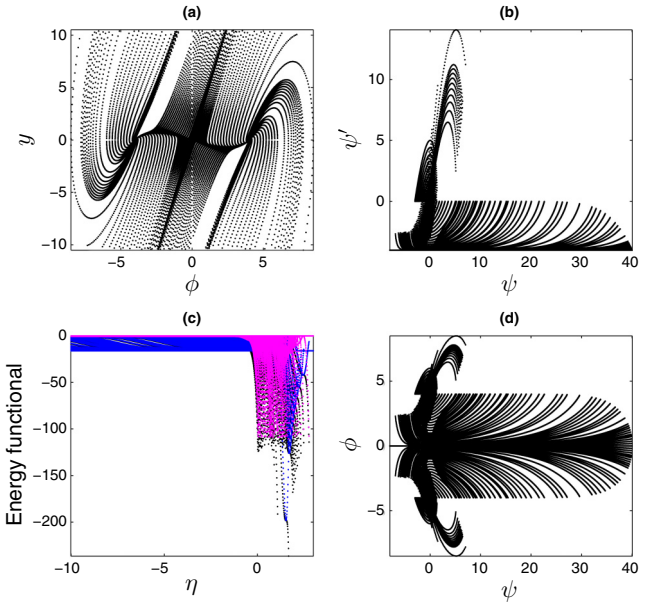

FIG. 3. (Color online) Phase features and energy functional of the system (3.13). The upper panels (a) and (b) depict the phase portraits of the system and the lower panel (c) deals with the energy densities of the corresponding traveling waveguide channels with the velocity $v = 2$ within a dissipation $s = 8$ and $K = -4$. In this panel, black, blue, and magenta represent the total energy, the potential energy, and the kinetic energy of the waves, respectively. Panel (d) presents the variations of observable ϕ with respect to ψ.

$\phi_0 = \pm\sqrt{2|Kv|}$. The behavior of the system around the points ϕ_0 is linearized as

$$X_\eta = AX, \tag{3.15}$$

with vector $X(\phi, y)$ and matrix A defined as

$$A = \begin{pmatrix} 0 & 1 \\ 2K/v & s/v \end{pmatrix}. \tag{3.16}$$

This linearization is similar to the one done near the origin (0,0) provided to set $2K = -K'$. In this case, the product $K'v$ is always positive definite. Consequently, the origin (0,0) is a saddle. Accordingly, we address the following discussion.

(i) $s > s_0$ with $s_0 = 2\sqrt{K'v} = 2\sqrt{2|Kv|}$. Remembering that velocity $v > 0$, vector X becomes infinite and does not tend to $(\phi_0,0)$. The equilibrium point is unstable. It is a divergent node. The phase portraits depict orbits diverging from the above point. We illustrate such a situation in Fig. 2. It is shown that the variations of observable ϕ can exhibit few profiles with vanishing tails. On the contrary, vanishing tails are not found among profiles of observable ψ which, because of the existence of the focal point in its phase portraits, present periodic shapes with varying amplitudes. As the waves propagate, their energy densities decrease up to a maximum rate of -120.

(ii) $s = s_0$. As $\eta \to +\infty$, vector X becomes infinite and does not tend to $(\phi_0,0)$. The equilibrium point is unstable. It is a divergent degenerated node. The phase portraits depict orbits diverging from the origin of the phase space but following a parabolic branch directed by the vector $(1,\lambda_0 = s_0/2v)$ near the equilibrium point. Figure 3 presents an illustrative situation where the existence of the saddle point (0,0) implies that observable ϕ can exhibit profiles with vanishing tails unlike those of the observable ψ showing periodic shapes with varying amplitudes. As the waves propagate, their energy densities decrease up to a maximum rate of -300.

(iii) $0 \leqslant s < s_0$. The vector X describes a spiral of asymptotical point O.

(a) If $s = 0$, the point $(\phi_0,0)$ is a summit or center. The phase portraits exhibit concentric cycles with $(\phi_0,0)$ as center. This is presented in Fig. 4. It is shown that the variations of observable ϕ can be periodic or localized. While vanishing tails are not found among profiles of observable ψ, the existence of homoclinic orbit through the origin of the phase portraits implies localized waves described by observable ϕ. This is observed through the variations of observable ϕ versus ψ depicting localized and harmonic loop shapes. As the waves propagate, their energy densities take constant values depending upon the initial data. For example, the lowest energy density is -16, corresponding to the origin (0,0).

(b) If $s \neq 0$, it appears that as $\eta \to +\infty$, vector X becomes infinite and does not tend to $(\phi_0,0)$. The equilibrium point is unstable. It is a divergent focal point. The phase portraits exhibit spirals winding around the equilibrium point within the direct sense while the motion occurs in the opposite direction. In Fig. 5, with the details presented in the caption, we present an illustrative situation. The existence of the saddle point (0,0) implies that observable ϕ can exhibit profiles with vanishing tails unlike those of the observable ψ showing periodic shapes with varying

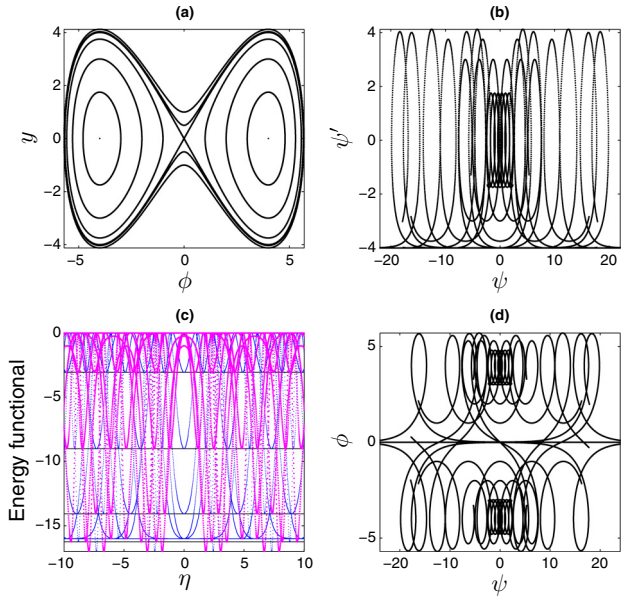

FIG. 4. (Color online) Phase features and energy functional of the system (3.13). The upper panels (a) and (b) depict the phase portraits of the system and the lower panel (c) deals with the energy densities of the corresponding traveling waveguide channels with the velocity $v = 2$ within a vanishing dissipation with $K = -4$. In this panel, black, blue, and magenta represent the total energy, the potential energy, and the kinetic energy of the waves, respectively. Panel (d) presents the variations of observable ϕ with respect to ψ.

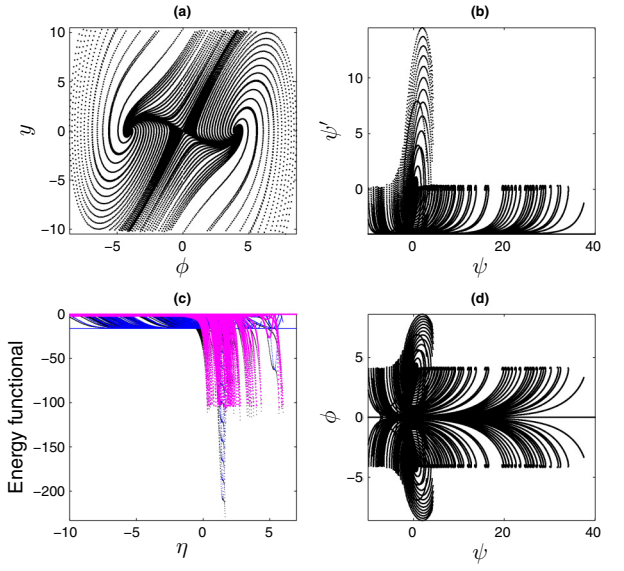

FIG. 5. (Color online) Phase features and energy functional of the system (3.13). The upper panels (a) and (b) depict the phase portraits of the system and the lower panel (c) deals with the energy densities of the corresponding traveling waveguide channels with the velocity $v = 2$ within a dissipation $s = 4$ and $K = -4$. In this panel, black, blue, and magenta represent the total energy, the potential energy, and the kinetic energy of the waves, respectively. Panel (d) presents the variations of observable ϕ with respect to ψ.

amplitudes. As the waves propagate, their energy densities decrease up to a maximum rate of -190.

From the above profiles, we have shown through the phase portraits that stable traveling waveguide channels can propagate within the ferrite provided the phase velocity v is positive-definite. This is hence corroborated by the confinement of their energy densities within the positive-definite η axis. Also, the inclusion of dissipation in the system contributes significantly to the decrease of the energy densities. Thus, the increase of the stability of the system from the viewpoint of the propagation of stable waveguide channels can be achieved with the introduction of dissipation within the system.

The phase portraits have shown that the moving structures globally belong to two families of waves, namely the periodic and the localized waves. Among the self-confined solitary waves, there is the loop-shaped waveguide channel described by the observable ϕ vs ψ. We aim at paying particular interest to the full nonlinear dynamics of such an excitation.

IV. SCATTERING BEHAVIOR OF THE LOCALIZED WAVEGUIDE CHANNELS: SOLITON STRUCTURE OF THE SYSTEM

In a first step, let us note the following. In account of the asymptotical boundary conditions $\lim_{X\to\infty} B = 0$ and $\lim_{X\to\infty} C_X = -(1+\mu)$ to Eq. (2.4), we consider the scale transformation given by

$$B \to (1+\mu)B, \quad C \to -(1+\mu)C,$$
$$T \to -T/(1+\mu), \quad X \to X. \tag{4.1}$$

Under the above transformation, the system given by Eq. (2.4) is invariant. In this section, the dependent variables B and C, and the independent variables T and X expressed below, are actually derived from Eq. (4.1), to which we refer when writing the genuine expressions of the original variables.

The invariant Eq. (2.4) with the transformation above, where conventionally space-time variables are written into their lowercase forms, possesses Lagrangian and Hamiltonian formulations as follows. With observables B and C regarded as two degrees of freedom of the system above, the Euler-Lagrange equation of motion of the system reads

$$\frac{\delta \mathcal{L}}{\delta B} = sB_x, \quad \frac{\delta \mathcal{L}}{\delta C} = 0, \tag{4.2}$$

where the Lagrangian $\mathcal{L}$ of the system is expressed as

$$\mathcal{L} = (B_x B_t + C_x C_t + B^2 C_x)/2. \tag{4.3}$$

From this Lagrangian formulation, the Hamiltonian of the system is given by

$$\mathcal{H} = (B_x B_t + C_x C_t)/2. \tag{4.4}$$

The expression of the Lagrangian above shows that it does not depend explicitly on time t. Consequently, the system under investigation is regarded as natural in such a way that its kinetic-like $\mathcal{T}$ and potential-like energy $\mathcal{V}$ densities can be derived seemingly. These quantities are then expressed as

$$\mathcal{T} = (B_x B_t + C_x C_t + B^2 C_x/2)/2,$$
$$\mathcal{V} = -B^2 C_x/4. \tag{4.5}$$

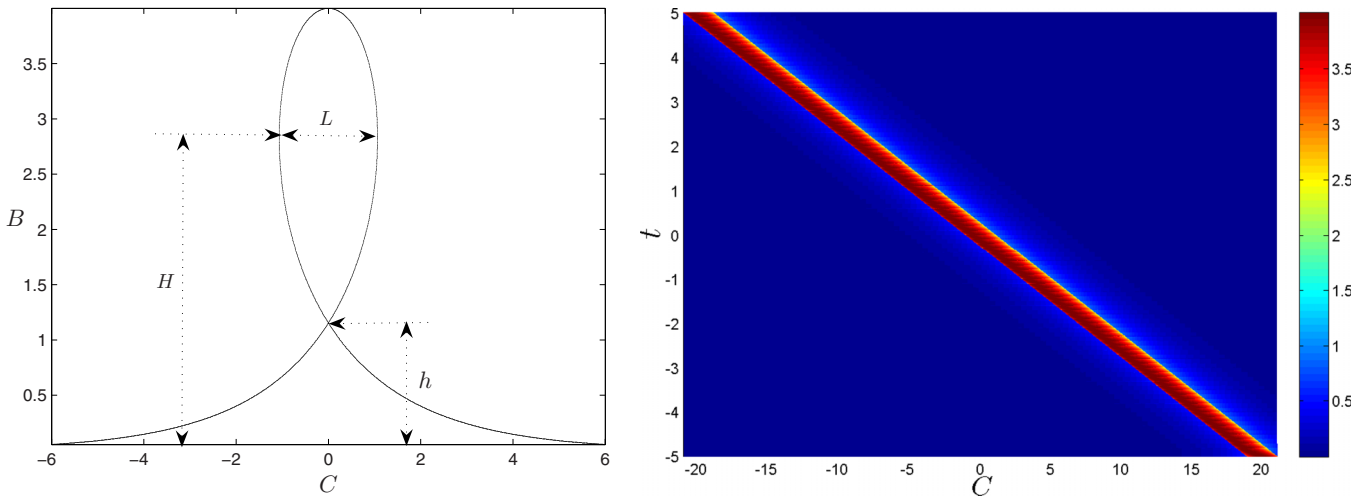

FIG. 6. (Color online) Multivalued single-waveguide channel solution to Eq. (2.4) in its invariant form. The snapshot is taken at initial time $t = 0$ and parameters are chosen arbitrarily as $A = 1$ and $\kappa = 0.5$. The panel on the right presents the density plot of such a traveling structure while showing a constant phase velocity of the wave propagation.

The energy-like functional of the system refers to the sum of its kineticlike $\mathcal{T}$ and potential-like energy $\mathcal{V}$ densities. Since the system is natural, we refer this sum to its total energy-like density represented by the Hamiltonian $\mathcal{H}$ above.

In order to tread into the scattering properties of the localized solutions, we pay particular interests to weak damping and we transform the system (2.4) into its bilinear form by means of the Hirota method [34]. As a result, we find

$$(D_x D_t + s D_x)GF = GF, \quad D_t^2 FF = G^2/2, \tag{4.6}$$

provided

$$B = G/F, \quad C = x - 2(\ln F)_t + x_0, \tag{4.7}$$

where the quantity x_0 is an arbitrary parameter. The symbol D_x, D_t refers to the Hirota's operators [34] with respect to the variable x, t, respectively. According to the usual procedure, the dependent functions G and F are expanded into suitable power series of a perturbation parameter ε. In this paper, in view of investigating the dynamics of localized excitations with vanishing tails, we arguably expand the functions G and F as follows:

$$\begin{aligned} G &= \varepsilon G_1 + \varepsilon^3 G_3 + \cdots, \\ F &= 1 + \varepsilon^2 F_2 + \varepsilon^4 F_4 + \cdots, \end{aligned} \tag{4.8}$$

where the functions G_i, F_i, $(i = 1,2,3,\ldots,)$ are expansion coefficients of the above series. Substituting this expansion into Eq. (2.4) and collecting the terms of each order of ε, we obtain the results presented below.

A. The one-soliton solution

The one-soliton solution to Eq. (4.6) is obtained from the following truncation:

$$G = \exp(\eta), \quad F = 1 + (\kappa^2/16)\exp(2\eta), \tag{4.9}$$

where the phase η is defined by

$$\eta = \kappa x + \omega t + \eta_0, \tag{4.10}$$

with constants κ and ω being wave number and frequency of the traveling wave and constant η_0 being an arbitrary parameter. According to Eq. (4.6), the dispersion relation reads $\omega\kappa = 1$ and the damping vanishes. For convenience, we arbitrarily choose $\kappa > 0$. Thus, the one-soliton solution expressed by Eq. (4.6) transforms to

$$B = 2\omega \mathrm{sech}\eta, \quad C = x - 2\omega(1 + \tanh\eta) + x_0. \tag{4.11}$$

Now, looking forward to comparing these one-soliton solutions with the ones given by Kraenkel, Merle, and Manna [26] through Eqs. (2.6) and (2.7), we need to consider the variable transformation given by Eq. (4.1). It hence comes that these expressions are similar provided the following relations:

$$\kappa = \overline{\kappa}, \quad \omega = 1/\overline{\kappa}, \quad \eta_0 = Z_0, \quad x_0 = C_0 - \frac{2}{\overline{\kappa}}(1 + \mu) \tag{4.12}$$

hold.

Figure 6 depicts the variations of the observable B with respect to variable C at $t = 0$. As observed, the shape of the profile is a loop propagating at a constant velocity ω^2 towards the negative-definite C axis. This velocity increases with the amplitude of the waves. Looking forward into the shape of this looplike solitary wave, we define the quantities L, H, and h standing for the maximum width of the loop, the height at which this occurs, and the height at which the crossover point occurs. This is all summarized in the above figure. We note that requiring symmetry in $(C - t)$ space, for the one-soliton solution above, we have chosen $x_0 = 2\omega$. Therefore, the crossover point will occur at $C = 0$ corresponding to $\eta = \eta_1$ so

$$\tanh\eta_1 = \kappa x_1/2. \tag{4.13}$$

Since the calculations are made at the initial time, when $\eta = \eta_1$, the height h is expressed as

$$h = 2\omega\sqrt{1 - \kappa^2 x_1^2/4}. \tag{4.14}$$

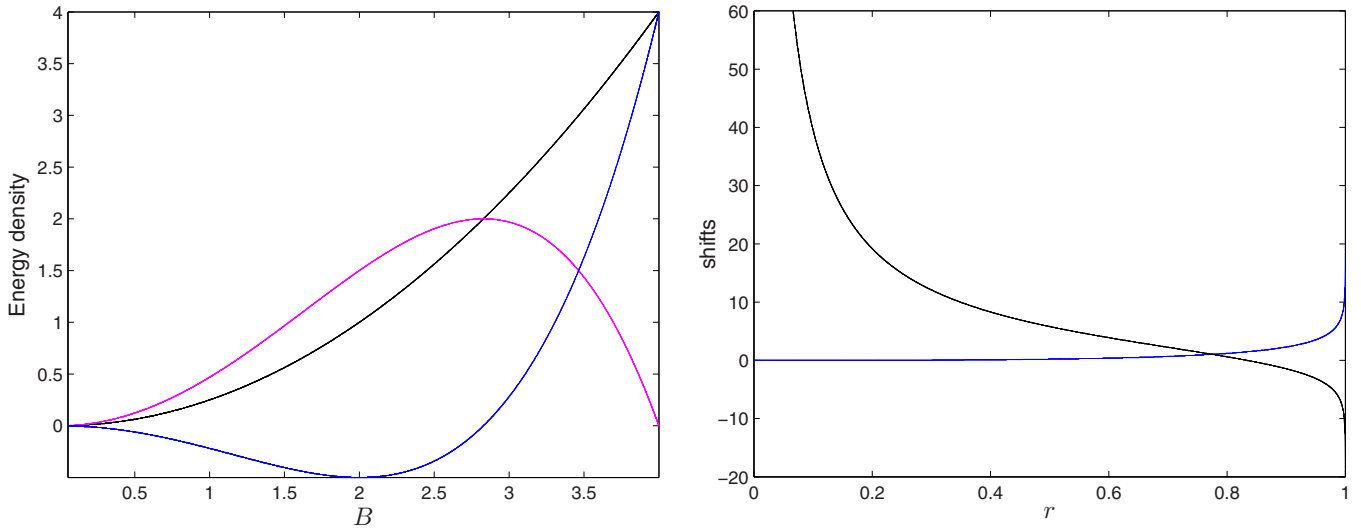

FIG. 7. (Color online) Energy functional of the multivalued single-waveguide channel solution to Eq. (2.4) in its invariant form. In this panel, black, blue, and magenta represent the total energy, the potential energy, and the kinetic energy densities of the wave, respectively. The panel on the right presents the shifts δ_1/ω_1 and δ_2/ω_2 of the interacting multivalued waveguide channels solutions to Eq. (2.4). Blue and black refer to shifts δ_1/ω_1 and δ_2/ω_2, respectively. From this panel, the shift δ_1 is always positive valued, meaning that the larger loop soliton is always shifted forwards by the interaction.

We solve Eq. (4.13) numerically and we obtain $\kappa x_1 = 1.9150$. With the details used to plot the one-soliton solution, we find $h = 1.1537$.

In order to derive the width L and height H, we have to solve the equation $1 - \kappa^2 B^2/2 = 0$. This leads to

$$H = \sqrt{2}\omega, \quad L = 2\omega[\sqrt{2} - \ln(\sqrt{2}+1)], \tag{4.15}$$

which numerically reads $H = 2.8284$ and $L = 2.1314$. The above numerical values vary with the wave parameters. From the expression of the amplitude of the solitary wave, i.e., 2ω, as the wave number κ increases, this amplitude decreases. Since the width L and the heights H and h are proportional to the amplitude of the wave, they also decrease with the wave number.

The evaluation of the energy density functional of this one-loop solitary wave is depicted in Fig. 7. As observed, the energy density $\mathcal{H}$ increases with the amplitude of the wave. The kinetic-like energy density of the wave increases until it reaches its maximum and then decreases further to zero. The potential-like energy density instead vanishes for $B \in \{0, H\}$ such that the part of the wave $0 \leqslant B \leqslant H$ is more stable than the upper part.

One further survey at this stage is to see whether the solitary wave above would actually behave as a particle, i.e., whether the term *soliton* can be coined to such a structure. We must now investigate the scattering properties of these kinds of waves within the interaction area.

B. The two-soliton solution

We truncate the expansion of Eq. (4.8) up to a fourth order of parameter ϵ. Therefore, we obtain

$$G = A_1 \exp(\eta_1) + A_2 \exp(\eta_2) + C_{12} \exp(\eta_1 + 2\eta_2) + C_{21} \exp(\eta_2 + 2\eta_1), \tag{4.16a}$$

$$F = 1 + B_{11} \exp(2\eta_1) + B_{22} \exp(2\eta_2) + B_{12} \exp(\eta_1 + \eta_2) + E_{12} \exp 2(\eta_1 + \eta_2), \tag{4.16b}$$

where

$$B_{11} = \frac{A_1^2}{16\omega_1^2}, \quad B_{22} = \frac{A_2^2}{16\omega_2^2}, \quad B_{12} = \frac{A_1 A_2}{2(\omega_1+\omega_2)^2}, \tag{4.17a}$$

$$C_{12} = \frac{A_1 B_{22}(\omega_1-\omega_2)^2}{(\omega_1+\omega_2)^2}, \; C_{21} = \frac{A_2 B_{11}(\omega_1-\omega_2)^2}{(\omega_1+\omega_2)^2}, \quad E_{12} = \frac{B_{11}B_{22}(\omega_1-\omega_2)^4}{(\omega_1+\omega_2)^4}, \tag{4.17b}$$

with $\eta_i = \kappa_i(x + t/\kappa_i^2) + \eta_{0i}$, $\kappa_i > 0$, $(i = 1,2)$. In order to investigate the nonlinear effects of the interaction, it is interesting to determine the shifts of the interacting waves. Thus, we assume that $\kappa_1 < \kappa_2$, meaning that the larger soliton is moving faster with the velocity c_1 than the smaller soliton of velocity $c_2 < c_1$. With such a hypothesis which does not break down the generality, the shifts δ_1 and δ_2 of these solitons expressed within the (C,t) coordinates are easily found as

$$\delta_1/\omega_1 = -4r + 2\ln\left(\frac{1-r}{1+r}\right), \quad \delta_2/\omega_2 = \frac{4}{r} + 2\ln\left(\frac{1-r}{1+r}\right), \tag{4.18}$$

where $r = \omega_2/\omega_1 = \kappa_1/\kappa_2$, $(0 < r < 1)$. The first term of the shift is due to two loops repelling, attracting each other, or traveling along another loop. The second terms show the shift caused by the nonlinear interaction between the solitons.

The plots of δ_1/ω_1 and δ_2/ω_2 as functions of the ratio r of the amplitudes of the individual smaller and larger solitons are

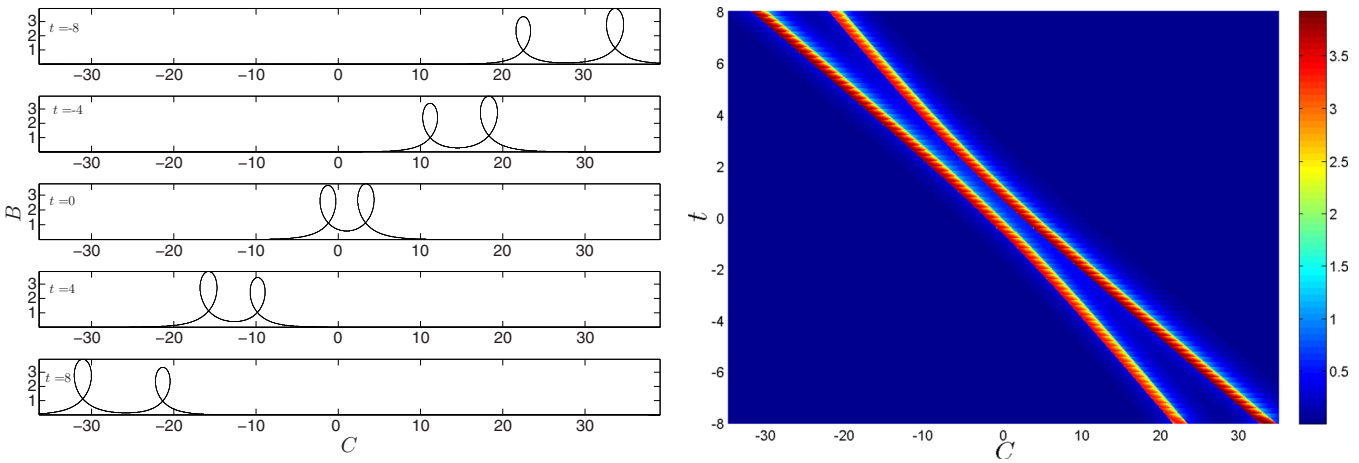

FIG. 8. (Color online) The interaction process for two multivalued waveguide channels solutions to Eq. (2.4) in its invariant form with $(A_1 = 1, \kappa_1 = 0.51)$ and $(A_2 = 1, \kappa_2 = 0.6)$ so the ratio $r = 0.85$. From this panel, the shift δ_2 is always negative valued, meaning that the smaller loop soliton is always shifted backwards by the interaction. The panel from right presents the density plot of the interaction process for two multivalued waveguide channels solutions to Eq. (2.4) with $(A_1 = 1, \kappa_1 = 0.51)$ and $(A_2 = 1, \kappa_2 = 0.6)$. From this depiction, the small soliton is shifted backwards, whereas the larger one is shifted forwards by the interaction.

shown in Fig. 7. It is seen that $\delta_1 > 0$ so the larger loop soliton is always shifted forwards by the interaction.

However, for the shift δ_2, we find that

(i) For $r = r_c$, where $r_c = 0.8336$ is the root of $2/r + \ln[(1-r)/(1+r)] = 0$, $\delta_2 = 0$. The smaller loop soliton is not shifted by the interaction.

(ii) For $0 < r < r_c$, $\delta_2 > 0$. The smaller loop soliton is shifted forwards.

(iii) For $0.8386 < r < 1$, $\delta_2 < 0$. The smaller loop soliton is shifted backwards.

Naturally, at first, it might seem that the behavior in (i) and (ii) contradicts conservation of "momentum." In fact, in a zero dissipation [Eq. (2.4)] can be transformed into the equation $\partial_C \partial_t B - \partial_C^2(B^3)/6 - B = 0$ such that after integration with respect to C, we find that $\int_{-\infty}^{+\infty} B dC = 0$. Also, by multiplying this equation by C and integrating with respect to C, we obtain $\int_{-\infty}^{+\infty} C B dC = 0$. Thus, in $(C - t)$ space, the "mass" of each soliton is zero, and momentum is conserved whatever δ_1 and δ_2 may be.

As an illustration of the previous analysis, a two-soliton solution feature is presented in Fig. 8 which describes the interaction between two similar amplitudes with the ratio $r = 0.85$. As we can see in this figure, the two single solitary waves seem to attract each other while moving to the left-hand side of the C axis. However, at the interaction area, it happens as the two waves repulse each other while exchanging amplitudes. As observed in previous Fig. 7, the smaller wave is shifted backwards while the larger is always shifted forwards. The density plot presented by Fig. 8 clearly represents such a phenomenon where we can see how a bundle line curves at the interaction area while changing its width at the final analysis. The computation of the energy densities of these waves is also depicted in Fig. 9(a). We see that in the zone $0 \leqslant B \leqslant 0.5826$ the interacting waves superimpose their profiles. The area is a stable zone where the potential-like energy density of the two-wave satisfies to $-0.8086 < \mathcal{V} < 0$. It corresponds to the center of the interacting area at time $t = 0$ where the waves do not overlap but present similar shapes (see Fig. 8). Within this zone, the densities $\mathcal{T}$ and $\mathcal{H}$ are monotone. For $B \in [0.5826, 1.9310]$, the two waves interact with each other but their shapes are no longer superimposed. In this area, the energy $\mathcal{V}$ decreases to -0.4423 while the densities $\mathcal{T}$ and $\mathcal{H}$ increase as multivalued functions. Now, for $B \geqslant 1.9310$, the interacting waves separate continuously, but the stable zone where the density $\mathcal{V}$ is still negative is $B \in [1.931, 2.686]$. In this interval, the energy $\mathcal{T}$ increases until it reaches its maximum while the total energy is monotone. It should be noted that the multivalued profile of the energy densities is an indication of the interaction features of two solitary waves. As a result of this interaction feature, the initial waves scatter elastically although exchanging amplitudes during the process. This property is characteristic of particles at the head-on collision

Another two-soliton feature is presented in Fig. 10 describing the interaction between two dissimilar amplitudes with the ratio $r = 0.5834$. As one can analyze the snapshots, the two solitary waves attract each other while moving to the left-hand side of the C axis. In contrast to the previous features, the head-on collision of the two loop solitons is attractive whereby the two solitons touch each other. Even if the two structures do not overlap, they superimpose their amplitudes at a given time. As depicted in Fig. 7, the smaller wave is shifted forwards as the larger one. The proper representations of these shifts are depicted in Fig. 10, which shows the density plots of the interacting solitons. These plots provide details regarding the scattering of the waves. As we can see in the figure, the initial bundle lines which are straight curve within the interacting area and recover their width at the end of analysis. In this interacting region, the shift of the larger soliton is smaller than that of the smaller soliton. Also, the energy densities of these waveguide channels are depicted in Fig. 9(b). In this figure, within the interval $B \in [0, 1.5]$, the interacting waves share the same amplitudes and profiles. This region is a stable one where the potential-like energy density of the two-wave satisfies to $-0.472 < \mathcal{V} < 0$. In this segment, the initial waves have the same profile and amplitudes, i.e., though they do not overlap. Accordingly, the energy densities $\mathcal{T}$ and $\mathcal{H}$ are monotone. For

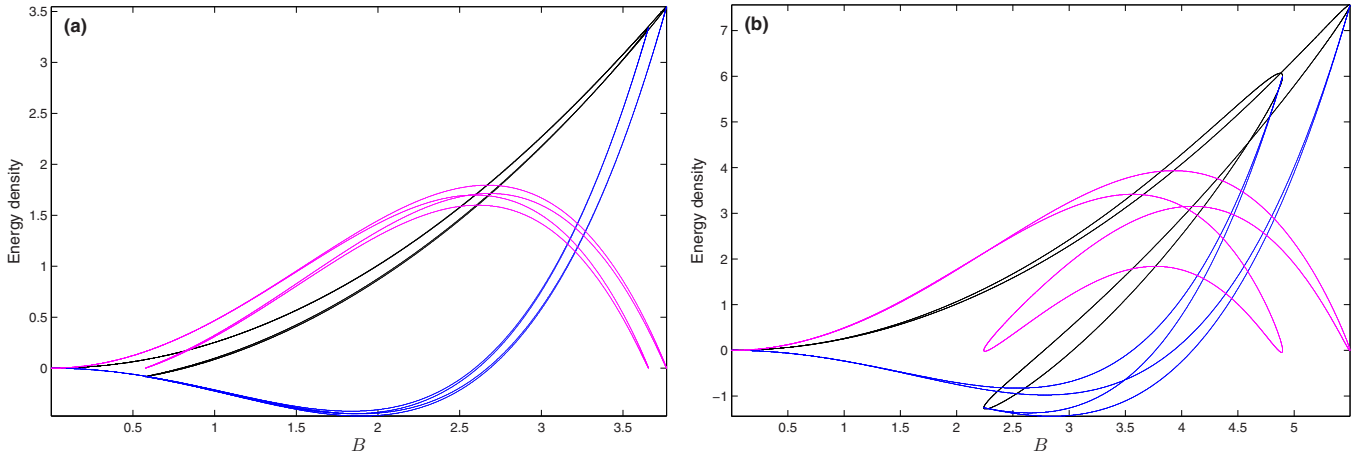

FIG. 9. (Color online) Panel (a) presents the energy density of interaction process for two multivalued waveguide channels solutions to Eq. (2.4) in its invariant form with $(A_1 = 1, \kappa_1 = 0.51)$ and $(A_2 = 1, \kappa_2 = 0.6)$ so the ratio $r = 0.85$. Panel (b) presents the energy density of interaction process for two multivalued waveguide channels solutions to Eq. (2.4) with $(A_1 = 1, \kappa_1 = 0.35)$ and $(A_2 = 1, \kappa_2 = 0.6)$ so the ratio $r = 0.5834$. In the figure, black, blue, and magenta represent the total energy, the potential energy, and the kinetic energy densities of the system, respectively.

$B \in [1.5,2]$, the two single waves interact mutually but with different amplitudes. In this area, the potential-like energy decreases to -0.7062 while densities $\mathcal{T}$ and $\mathcal{H}$ continue to increase. After the interaction, the initial soliton continue their propagation trip for $B \geqslant 2$. Nonetheless, the stable part of their shape is obtained where the potential-like energy density is negative valued, i.e., $B \in [3.563,4.098]$. Within this zone, the multivalued density $\mathcal{T}$ increases until it reaches its maxima and further decreases in a peculiar manner. On contrary to the density $\mathcal{T}$, the multivalued energy density $\mathcal{H}$ can take negative values particularly in the region where the potential $\mathcal{V}$ is negative valued.

Still paying interest to the interacting waves with positive-definite amplitudes, we consider the case where the ratio r is small. For example $r = 1/3$. This is another case of dissimilarity of amplitudes. The illustration is made in Fig. 11 which presents two solitons moving towards negative-definite C axis where the small wave travels along the larger one anticlockwise before separating each other at the final analysis while recovering their initial shapes, respectively. During this process, the two solitons shift forwards, i.e., $\delta_1 > 0$ and $\delta_2 > 0$. But, graphically, since the large soliton has an amplitude that is relatively greater than that of the small one, the large soliton seems to be unmoving. This phenomenon is depicted in Fig. 11, which presents the density plot of the interacting waves. Evaluating the energy densities of these structures, we follow the same procedure as in the previous figure and we plot in Fig. 12(a) the densities $\mathcal{T}$, $\mathcal{V}$, and $\mathcal{H}$. This is to characterize the features of the interacting area. As we can see in this figure, for $B \in [0,4]$, the larger soliton overlaps the small one, which corresponds here to the small soliton traveling along the large one. In this scale, the potential-like energy $\mathcal{V}$

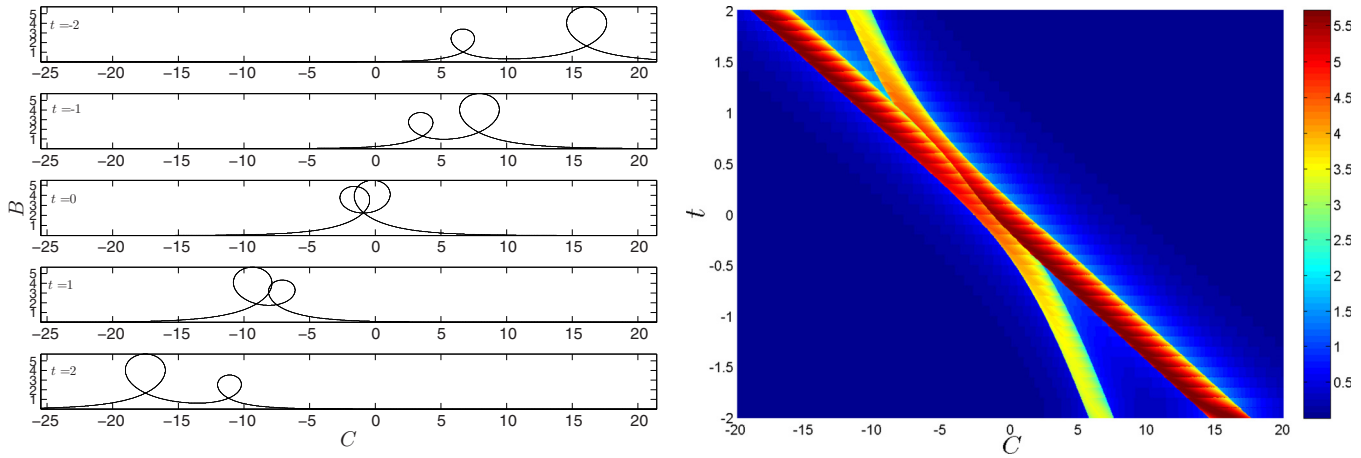

FIG. 10. (Color online) The interaction process for two multivalued waveguide channels solutions to Eq. (2.4) in its invariant form with $(A_1 = 1, \kappa_1 = 0.35)$ and $(A_2 = 1, \kappa_2 = 0.6)$ so the ratio $r = 0.5834$. From this panel, the shift δ_2 is always positive valued, meaning that the smaller loop soliton is shifted forwards by the interaction. The panel from right presents the density plot of the interaction process for two multivalued waveguide channels solutions to Eq. (2.4) with $(A_1 = 1, \kappa_1 = 0.35)$ and $(A_2 = 1, \kappa_2 = 0.6)$. From this depiction, the smaller and larger soliton are both shifted forwards by the interaction.

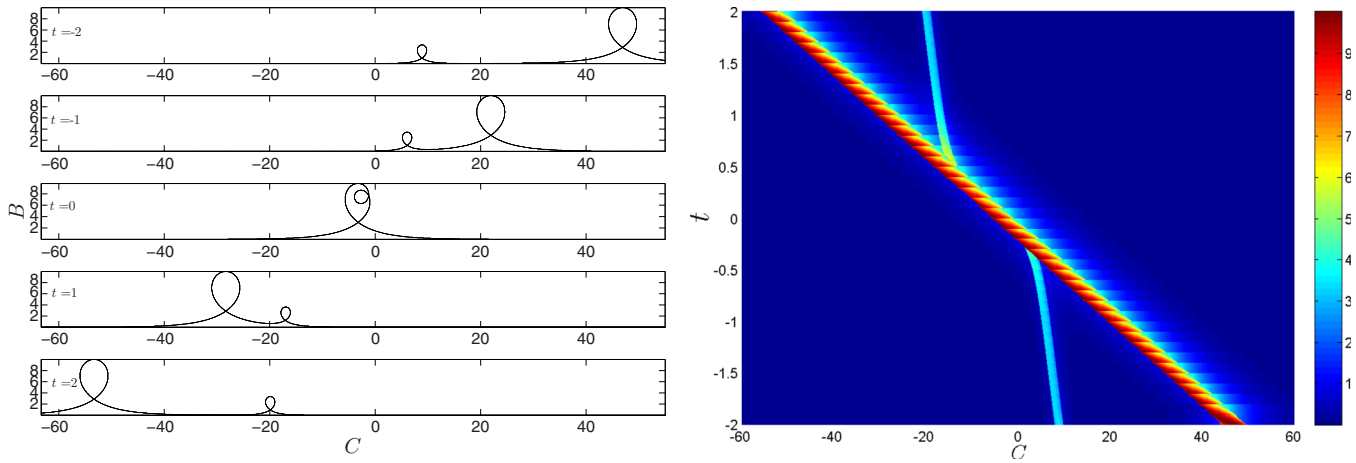

FIG. 11. (Color online) The interaction process for two multivalued waveguide channels solutions to Eq. (2.4) with $(A_1 = 1, \kappa_1 = 0.2)$ and $(A_2 = 1, \kappa_2 = 0.6)$ so the ratio $r = 0.3334$. From this panel, the shift δ_2 is always positive valued, meaning that the smaller loop soliton is shifted forwards by the interaction. The panel on the right presents the density plot of the interaction process for two multivalued waveguide channels solutions to Eq. (2.4) with $(A_1 = 1, \kappa_1 = 0.2)$ and $(A_2 = 1, \kappa_2 = 0.6)$. From this depiction, the smaller and larger solitons are both shifted forwards by the interaction.

is negative valued and satisfies to $-2.649 < \mathcal{V} < 0$, showing that these amplitudes are the stable ones. Simultaneously, the energy densities $\mathcal{T}$ and $\mathcal{H}$ increase with amplitude B. For $B \in [4, 4.716]$, the two single waves interact mutually but begin to separate from each other. In this range, the potential energy $\mathcal{V}$ decreases to -2.894 where densities $\mathcal{T}$ and $\mathcal{H}$ increase. Following this step, the interacting waves evolve with clearly separated shapes but it appears that in this zone of $B \geqslant 4.716$, while the multivalued energy $\mathcal{T}$ increases and further decreases, the multivalued total energy density varies in a peculiar scheme. Nonetheless, the stable part of their shape of the two-soliton is numerically evaluated as the range $[6.561, 7.897]$. Within this range, total energy $\mathcal{H}$ and the kinetic $\mathcal{T}$ can take negative values, in contrast to the previous cases. However, these constitute useful indications of the stability of this part of the two-soliton solution.

We note that the quantity $(-B)$ is also a solution to Eq. (2.4). The case of a positive-definite observable has been surveyed above. Now we combine the two cases by studying the interaction between a loop and an antiloop soliton. We consider the interaction between two dissimilar amplitudes where the larger amplitude refers to a soliton and the lower amplitude stands for an antisoliton, i.e., a soliton with an algebraically negative-definite amplitude. The details are presented in the caption to Fig. 13. With these details, the shifts expressed by Eq. (4.18) are positive valued, meaning that, during the process of interaction, the two waves shift forwards. As observed in the figure, during the scattering process, the antiloop soliton travels anticlockwise along the loop soliton before being shifted forwards at the final analysis. This phenomenon is remarkable and is actually characteristic of the interaction between such waves no matter how dissimilar or similar their

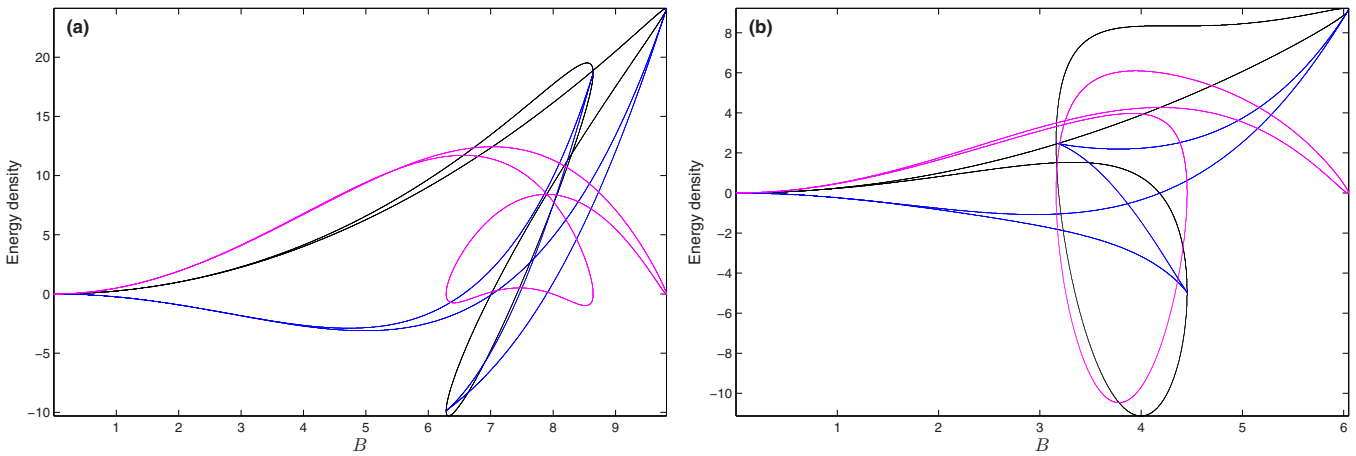

FIG. 12. (Color online) Panel (a) presents the energy density of interaction process for two multivalued waveguide channels solutions to Eq. (2.4) in its invariant form with $(A_1 = 1, \kappa_1 = 0.2)$ and $(A_2 = 1, \kappa_2 = 0.6)$ so the ratio $r = 0.3334$. Panel (b) presents the energy density of interaction process for two multivalued waveguide channels solutions to Eq. (2.4) in its invariant form with $(A_1 = 1, \kappa_1 = 0.35)$ and $(A_2 = -1, \kappa_2 = 0.6)$ so the ratio $r = 0.5834$. In the figure, black, blue, and magenta represent the total energy, the potential energy, and the kinetic energy densities of the system, respectively.

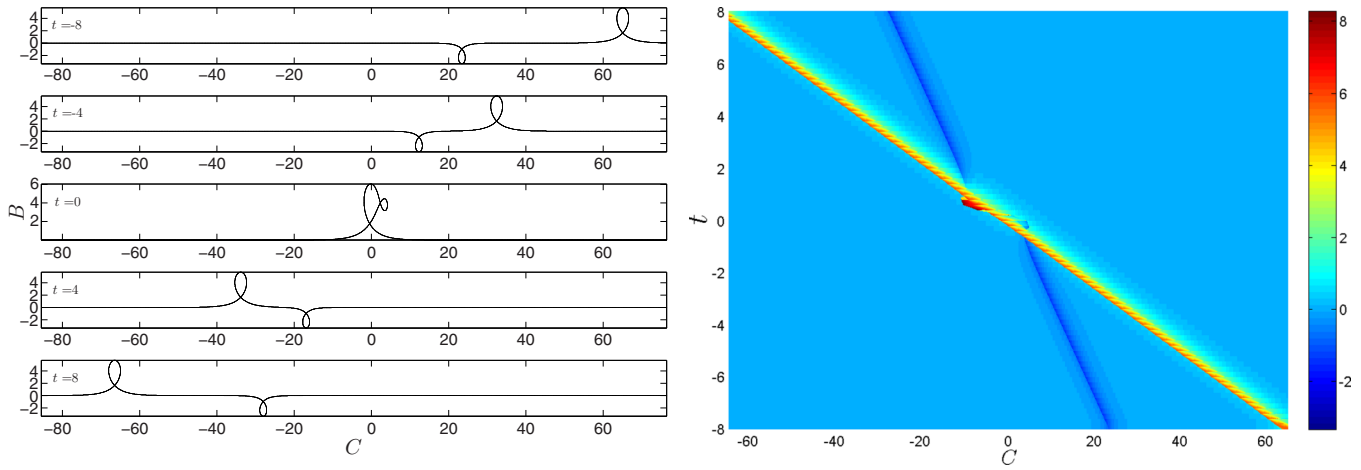

FIG. 13. (Color online) The interaction process for two multivalued waveguide channels solutions to Eq. (2.4) with $(A_1 = 1, \kappa_1 = 0.35)$ and $(A_2 = -1, \kappa_2 = 0.6)$ so the ratio $r = 0.5834$. From this panel, the shift δ_2 is always positive valued, meaning that the smaller loop soliton is shifted forwards by the interaction. The panel from right presents the density plot of the interaction process for two multivalued waveguide channels solutions to Eq. (2.4) with $(A_1 = 1, \kappa_1 = 0.35)$ and $(A_2 = -1, \kappa_2 = 0.6)$. From this depiction, the two solitons are both shifted forwards by the interaction.

amplitudes are. A graphical representation of the shifts is presented in Fig. 13, which depicts the density plots of the interacting waves. In this figure, since the amplitude of the loop soliton is greater than that of the antiloop soliton, the larger soliton seems to observe a zero phase shift. In the interacting area, the density plots show how the antiloop soliton travels along the soliton. This interacting area appears as the zone where the straight rope characterizing the soliton and the soft string referring to the antisoliton fasten together. Evaluating the energy functional of this kind of two-soliton, we plot the densities $\mathcal{V}, \mathcal{T}$, and $\mathcal{H}$ in the plane presented in Fig. 12(b). From these plots it is shown that for amplitudes $B \in [0, 1.859]$, there is a one-loop shape which corresponds to the overlapping of the antiloop soliton. Such an overlapping has a particular meaning of the antisoliton traveling around the soliton during the propagation in the scattering area. In this range of amplitude, the potential energy $\mathcal{V}$ satisfies to $-0.6875 < \mathcal{V} < 0$ and the other densities increase with the amplitude B. Still within the interacting area, for $B \in [1.859, 2.168]$ the two waves begin to separate each from other. In this zone, the densities $\mathcal{T}$ and $\mathcal{H}$ become multivalued while increasing with B and the potential energy $\mathcal{V}$ decreases to -0.8505. This part of amplitudes denotes a stable two-wave. For $B > 2.168$, the interacting waves evolve with clearly separated shapes. Nonetheless, the stable part of the amplitudes of the two-loop is obtained in the range $B \in [2.168, 4.453]$, within which the multivalued densities $\mathcal{T}$ and $\mathcal{H}$ show both negative and positive values.

V. PHYSICAL IMPLICATIONS OF THE SOLUTIONS

In order to provide some physical implications of the results obtained in this work, we should recall that the dimensionless quantity B refers to the the magnetization within the ferrite. Thus, the magnetization in the ferrite evolves as a traveling wave with finite tails. Since it can be positive valued or negative valued, it then describes bright and dark solitary waves with pulselike profiles. These solitary waves interact mutually through elastic process. Thus, within the ferrite, in a fast magnetization process while loading the magnetic memory devices, we can send simultaneously data inputs in terms of nonlinear excitations in the magnet which, as a result, will interact together to retrieve their initial properties at the end of the process. Also, in a remagnetization process, the ferromagnet can support the propagation of some solitary waves sent in the structure sequently to produce typical periodic or doubly periodic waves. Thus, by propagating a sequence of single-valued waveguide channels of different amplitudes such as humplike soliton solutions in the ferrite after some time intervals, the data inputs will undergo a fast magnetization process within the magnetic memory device while empowering the system with a great and efficient storage capacity.

In another hand, from the expression of the observable C, it is possible to evaluate the profile of the external magnetic field. Discussing the physical structure of the solutions in terms of the observables **M** and **H**, the magnetization and the magnetic field behave differently in the ferrite. In fact, during the magnetic relaxation process where the magnetization and magnetic field are restored to their equilibrium positions, while the magnetization describes a bright soliton, the magnetic field behaves, in contrast, as a dark soliton. Fundamentally, within the region of the ferrite where the magnitude of the external magnetic field decreases significantly, the number of magnetic dipoles increases. This is particularly very important in the magnetic information storage and data process elements in micromagnetic structure of ferromagnets. It should, however, be noted that the propagation of solitons in the ferrite is made possible under the assumption that the slab is magnetized to saturation by an in-plane external magnetic field directed along the transverse direction perpendicularly to the propagation axis. Under such an assumption, through a magnetic storage process in ferrite devices such as yttrium iron garnet films [35], we can send in the medium some perturbations of the external magnetic fields in the form of nonlinear excitations of dark types. These structures will then interact elastically, that is, there is scattering without the structural alteration of the initial magnetic inputs.

VI. SUMMARY

In this work, we have investigated the fast near-adiabatic magnetization dynamics of a nonconducting ferromagnetic slab from the viewpoint of a short-wavelength approximation. At the starting point of the study, we have considered a one-dimensional slab lying in the x axis, the direction of the propagation of waves. This ferromagnetic insulator known as ferrite [26] is magnetized to saturation by an in-plane external field $\mathbf{H}_0^{\infty}$ directed along the y axis, in the absence of any eddy currents in view of allowing electromagnetic wave propagation. We have chosen a thick-enough condition at the film boundaries to ensure a homogeneous magnetization over the ferrite. We have also assumed that the crystalline and surface anisotropy of the sample are negligible. The LLG equation [29] actually stands to be the simplest conceivable model to describe the fast near-adiabatic magnetization dynamics of a ferromagnet. Using the full set of Maxwell's equations associated to the previous dynamical equation [29], a governing coupled system of equations with dissipation has been derived and addressed for the propagation of nonlinear electromagnetic short waves in ferrites [26].

Looking forward to surveying the integrability properties of the above coupled system, we have investigated the phase portraits of the system combined to the Hirota's bilinearization [34] among other methods of study. This initial value problem of the system has provided a whole depiction of the dynamics of the system while revealing the existence of miscellaneous traveling waveguide excitations supported by the system. The Hirota's bilinearization [34] has, on the other side, provided a whole analysis of the interaction of localized waves while characterizing the head-on collision. Indeed, alongside the phase portraits of the system, we have also computed its energy functional through the total energy and the kinetic and potential energy densities. Prior to the numerical analysis of the subject, we delved into the analytical structure of the initial value problem. We found that under some considerations, the system possesses one or three equilibrium points behaving as nodes or saddle or focal points. The depiction of the energy densities of the traveling waveguide channels have shown that the stable excitations are those propagating with a positive-definite velocity, that is, waves moving to the positive-valued propagating axis. Paying particular interest to the localized waves, we have focused our interests on the structures moving with vanishing tails. With the help of Hirota's method [34], we have investigated the dynamics of the magnetization with respect to an implicit function related to the external magnetic field. This investigation has revealed the soliton structure of the magnet under study. We have unearthed a typical type of soliton solutions with looplike shapes interacting elastically in the medium. We have also provided some details about such a profile. We have computed the shifts of the interacting waves characterizing the nonlinear scattering and the head-on collision, and we found that the larger soliton is always shifted forwards during the interaction. Investigating the interaction features in detail, we found that when the amplitudes of the interacting waves are "dissimilar," the waves attract each other in such a way that the smaller soliton travels along the larger one before being shifted at the end of the analysis. When the amplitudes are "similar," the initial waves repulse or seem to exchange amplitudes. When there is interaction between a soliton and an antisoliton solution, it is always the antisoliton which travels along the soliton before being shifted, no matter how dissimilar or similar their amplitudes are. Globally, it appears as there exists a critical value of the ratio of the interacting waves at which the collision process changes its characteristic features. Alongside these interacting features, we have also computed their energy functional, which is useful in assessing the stability of the interacting waves.

As a physical implication of the results, within the ferrite, in a fast magnetization process while loading the magnetic memory devices, we can send simultaneously data inputs in terms of nonlinear excitations in the magnet. These excitations will interact together elastically to retrieve their initial properties at the end of the process. In addition, during the magnetic relaxation process where the magnetization and magnetic field are restored to their equilibrium positions, while the magnetization describes a bright soliton, the magnetic field behaves, in contrast, as a dark soliton. Fundamentally, within the region of the ferrite where the magnitude of the external magnetic field decreases significantly, the number of magnetic dipoles increases. This is particularly very important in terms of the magnetic information storage and data process elements in the micromagnetic structure of ferromagnets.

Moreover, the range of validity of the LLG equation had previously been established by Brown [36] through the description of a magnetic moment coupled to a heat bath and treated as a Brownian particle described by the slow degrees of freedom of angular types. Since the early 2000s [37], important experimental advances regarding the very short time-resolved response of the magnetization below the limit proposed by Brown [36] have been reported. Very recently, the dynamical equation for magnetization has been reconsidered by enlarging the phase space of the ferromagnetic degrees of freedom to the angular momentum [23]. The generalized LLG equation that includes inertial terms, and the corresponding Fokker-Planck equation, are then derived in the framework of mesoscopic nonequilibrium thermodynamics theory. It is obvious that the introduction of such an inertial regime offers new opportunities for the implementation of ultrafast magnetization switching in magnetic devices. The question remains whether this generalized LLG equation would furnish further information about the dynamics of polaritons where inertial terms are regarded. We aim to investigate such a problem in a separate paper.

In addition, it has been shown that the inclusion of the spin-torque term in the LLG equation provides more information about the magnetization relaxation processes described by the radiation-spin interaction where the radiation field is produced by the magnetization precessional motion itself [38]. We believe that the investigation of such a system alongside the inclusion of the spin-torque term in the generalized LLG equation above [23], within the framework of the formalism elaborated in this paper, would be worth studying.

ACKNOWLEDGMENTS

The authors express their sincere thanks to the anonymous referees for their critical comments and appropriate suggestions, which have made this paper more precise and readable.

V.K.K. is very grateful for the hospitality and the financial supports in publication from the Abdus Salam International Centre for Theoretical Physics (ICTP, Trieste, Italy) where part of the present work has been finalized.

[1] P. L. Christiansen, M. P. Sorensen, and A.C. Scott, *Nonlinear Science at the Dawn of the 21st Century* (Springer, Berlin, 2000); A. Hasegawa, *Massive WDM and TDM Soliton Transmission* (Kluwer Academic, Dordrecht, 2000); J. R. Taylor, ed., *Optical Solitons: Theory and Experiment* (Cambridge University Press, Cambridge, 1992); N. N. Akhmediev and A. Ankiewicz, *Solitons: Nonlinear Pulses and Beams* (Chapman & Hall, London, 1997); J. M. Dudley and J. R. Taylor, eds., *Optical Fiber Supercontinuum Generation* (Cambridge University Press, Cambridge, 2010); J. C. Travers, J. Opt. **12**, 113001 (2010); P. Holzer, W. Chang, J. C. Travers, A. Nazarkin, J. Nold, N. Y. Joly, M. F. Saleh, F. Biancalana, and P. S. J. Russell, Phys. Rev. Lett. **107**, 203901 (2011).

[2] C. Rebbi and G. Soliani, *Solitons and Particles* (World Scientific, Singapore, 1984).

[3] N. S. Manton, Nonlinearity **21**, T221 (2008).

[4] L. M. Kovachev, Physica D **190**, 78 (2004).

[5] L. M. Kovachev, Int. J. Math. Math. Sci. **2004**, 1403 (2004).

[6] Yu. P. Rybakov and B. Saha, Ann. Fond. Louis de Broglie **26**, 381 (2001).

[7] A. M. Kosevich, Physica D **41**, 253 (1990).

[8] T. L. Belyaeva, V. N. Serkin, C. Hernandez-Tenorio, and F. Garcia-Santibanez, J. Mod. Opt. **57**, 1087 (2010).

[9] H. K. Moffatt, J. Fluid Mech. **35**, 117 (1969).

[10] H. K. Moffatt, J. Fluid Mech. **106**, 27 (1981).

[11] R. Ricca and M. Berger, Phys. Today **49**, 28 (1996).

[12] I. I. Smalyukh, Y. Lansac, N. A. Clark, and R. P. Trivedi, Nat. Mater. **9**, 139 (2010).

[13] U. Tkalec, M. Ravnik, S. Copar, S. Zumer, and I. Musevic, Science **333**, 62 (2011).

[14] M. R. Dennis, R. P. King, B. Jack, K. O'Holleran, and M. J. Padgett, Nat. Phys. **6**, 118 (2010).

[15] A. F. Rañada, J. Phys. A **23**, L815 (1990).

[16] W. T. M. Irvine and D. Bouwmeester, Nat. Phys. **4**, 716 (2008).

[17] W. T. M. Irvine, J. Phys. A **43**, 385203 (2010).

[18] Y. Kawaguchi, M. Nitta, and M. Ueda, Phys. Rev. Lett. **100**, 180403 (2008).

[19] H. Kedia, I. Bialynicki-Birula, D. Peralta-Salas, and W. T. M. Irvine, Phys. Rev. Lett. **111**, 150404 (2013).

[20] E. J. Parkes, Chaos Solitons Fractals **38**, 154 (2008); V. K. Kuetche, T. B. Bouetou, and T. C. Kofane, J. Phys. Soc. Jpn. **76**, 024004 (2007); Y. Matsuno, *ibid.* **76**, 084003 (2007).

[21] S. Stalin and M. Senthilvelan, Phys. Scr. **86**, 015006 (2012); Y. Matsuno, J. Math. Phys. **49**, 073508 (2008); Y. Yao and Y. Zeng, J. Phys. Soc. Jpn. **80**, 064004 (2011); J. C. Brunelli and S. Sakovich, J. Math. Phys. **54**, 012701 (2013).

[22] S. Ishizaka and K. Nakamura, J. Mag. Mag. Mat. **210**, 15 (2000).

[23] M. C. Ciornei, J. M. Rubi, and J. E. Wegrowe, Phys. Rev. B **83**, 020410 (2011).

[24] M. Fähnle, D. Steiauf, and C. Illg, Phys. Rev. B **84**, 172403 (2011).

[25] Y. B. Bazaliy, B. A. Jones, and S. C. Zhang, Phys. Rev. B **57**, R3213 (1998).

[26] R. A. Kraenkel, M. A. Manna, and V. Merle, Phys. Rev. E **61**, 976 (2000).

[27] H. Leblond and M. Manna, Phys. Rev. E **50**, 2275 (1994).

[28] A. K. Zvezdin and A. F. Popkov, Sov. Phys. JETP **57**, 350 (1983); A. N. Slavin and I. V. Rojdestvenski, IEEE Trans. Magn. **30**, 37 (1994).

[29] T. L. Gilbert, IEEE Trans. Magn. **40**, 3443 (2004); Phys. Rev. **100**, 1243 (1955).

[30] J. Z. Sun, J. Mag. Mag. Mat. **202**, 157 (1999).

[31] B. V. Waeyenberge, A. Puzic, H. Stoll, K. W. Chou, T. Tyliszczak, R. Hertel, M. Fähnle, H. Brückl, K. Rott, G. Reiss, I. Neudecker, D. Weiss, C. H. Back, and G. Schütz, Nature (London) **444**, 461 (2006).

[32] B. Koopmans, G. Malinowski, F. D. Longa, D. Steiauf, M. Fähnle, T. Roth, M. Cinchetti, and M. Aeschlimann, Nat. Mater. **9**, 259 (2012).

[33] J. Kevorkian and J. D. Cole, *Multiple Scale and Singular Perturbation Methods* (Springer, New York, 1996).

[34] R. Hirota, *Direct Methods in Soliton Theory* (Cambridge University Press, Cambridge, 2004).

[35] P. De Gasperis, R. Marcelli, and G. Miccoli, Phys. Rev. Lett. **59**, 481 (1987); B. A. Kalinikos, N. G. Kovshikov, and A. N. Slavin, Phys. Rev. B. **42**, 8658 (1990).

[36] W. F. Brown Jr., Phys. Rev. **130**, 1677 (1963).

[37] A. V. Kimel *et al.*, Nature (London) **435**, 655 (2005); E. Beaurepaire, J. C. Merle, A. Daunois, and J. Y. Bigot, Phys. Rev. Lett. **76**, 4250 (1996); C. D. Stanciu, F. Hansteen, A. V. Kimel, A. Kirilyuk, A. Tsukamoto, A. Itoh, and T. Rasing, *ibid.* **99**, 047601 (2007).

[38] J. Ho, F. C. Khanna, and B. C. Choi, Phys. Rev. Lett. **92**, 097601 (2004).